



HAL
open science

High frequency analysis of the efficiency of a local approximate DtN2 boundary condition for prolate spheroidal-shaped boundaries

Hélène Barucq, Rabia Djellouli, Anne-Gaëlle Saint-Guiron

► **To cite this version:**

Hélène Barucq, Rabia Djellouli, Anne-Gaëlle Saint-Guiron. High frequency analysis of the efficiency of a local approximate DtN2 boundary condition for prolate spheroidal-shaped boundaries. [Research Report] RR-7137, INRIA. 2009, pp.38. inria-00438845v2

HAL Id: inria-00438845

<https://inria.hal.science/inria-00438845v2>

Submitted on 16 Dec 2009

HAL is a multi-disciplinary open access archive for the deposit and dissemination of scientific research documents, whether they are published or not. The documents may come from teaching and research institutions in France or abroad, or from public or private research centers.

L'archive ouverte pluridisciplinaire **HAL**, est destinée au dépôt et à la diffusion de documents scientifiques de niveau recherche, publiés ou non, émanant des établissements d'enseignement et de recherche français ou étrangers, des laboratoires publics ou privés.

***High frequency analysis of the efficiency of a local
approximate DtN2 boundary condition for prolate
spheroidal-shaped boundaries***

Hélène Barucq — Rabia Djellouli — Anne-Gaëlle Saint-Guirons

N° 7137

December 2009

Domaine 1



***rapport
de recherche***

High frequency analysis of the efficiency of a local approximate DtN2 boundary condition for prolate spheroidal-shaped boundaries

Hélène Barucq^{* †}, Rabia Djellouli^{‡ §}, Anne-Gaëlle Saint-Guirons^{¶ * †}

Domaine : Mathématiques appliquées, calcul et simulation
Équipe-Projet Magique 3D

Rapport de recherche n° 7137 — December 2009 — 37 pages

Abstract: The performance of the second order local approximate DtN boundary condition suggested in [4] is investigated analytically when employed for solving high-frequency exterior Helmholtz problems. This study proves that, in the high frequency regime, the reflected waves at the artificial boundary decay faster than $1/(ka)^{15/8}$ where k is the wavenumber and a is the semi-major axis of this boundary. Numerical results illustrate the accuracy and the efficiency of the proposed absorbing boundary condition when used for solving acoustic scattering problems in a domain-based formulation.

Key-words: acoustic scattering problems, prolate spheroidal coordinates, prolate spheroidal-shaped boundaries, absorbing boundary conditions, DtN operator

* INRIA Futurs Research Center Team-Project Magique3D

† Laboratoire de Mathématiques Appliquées, CNRS UMR 5142, Université de Pau et des Pays de l'Adour, IPRA-Avenue de l'Université, 64013 Pau, France

‡ Department of Mathematics, California State University Northridge, CA 91330-8313, USA

§ INRIA Futurs Research Center Associate Team Magic

¶ Basque Center for Applied Mathematics, Bizkaia Technological Park, Building 500, 48160 Derio, Spain

Performance de la condition DtN2 pour des frontières elliptiques en régime haute fréquence

Résumé : Nous étudions analytiquement la performance de la condition locale approchée DtN2 proposée dans [4] pour résoudre les problèmes extérieurs de Helmholtz. Nous démontrons que l'amplitude des ondes réfléchies par la frontière artificielle extérieure décroît plus vite que $1/(ka)^{15/8}$ où k est le nombre d'onde et a le demi-axe principal de cette frontière. De plus, nous présentons des résultats numériques qui illustrent la capacité de cette condition aux limites absorbante à résoudre les problèmes de scattering efficacement et avec une grande précision.

Mots-clés : Problèmes de scattering, frontières prolates sphéroïdales, conditions absorbantes, opérateur DtN

1 Introduction

The development of efficient solution methodologies for solving scattering problems is very important to many applications such as sonar, radar, medical imaging, geophysical exploration, non destructive testing, etc. This is a very challenging problem because of two difficulties that one need to address: (a) the discretization issue related to the wavenumber, especially in the high frequency regime, and (b) the unboundness nature of the computational domain (see, for example, the recent monograph [13] and the references therein) . In this work, we focus on the second aspect of this problem and we consider one of the basic problem in the scattering theory: the scattering of time-harmonic acoustic waves by a bounded impenetrable obstacle [7]. The computation of the corresponding acoustic scattered field when using finite element methods, requires first to reformulate this class of problems in a finite domain by surrounding the scatterer by an artificial boundary. The main difficulty here is the construction of a simple but reliable as well as cost-effective absorbing boundary condition for representing the far-field behavior of the scattered field on the prescribed artificial boundary. Various absorbing boundary conditions have been suggested for over seventy years to address this challenging and important issue, and the quest for efficient nonreflecting conditions is still ongoing (see, for example, the latest review by Turkel in [22]).

Recently, a new class of absorbing boundary conditions called local approximate DtN absorbing boundary conditions (DtN) has been proposed to be applied on exterior artificial prolate spheroidal-shaped boundaries [4]. Unlike the standard approximate local DtN boundary conditions that are restricted to circular- or spherical-shaped boundaries (see [10],[11]), the proposed conditions are applicable to exterior elliptical- or prolate spheroidal-shaped boundaries that are more suitable for surrounding elongated scatterers because they yield to smaller computational domains. These absorbing boundary conditions are designed to be exact for the first modes. They can be easily incorporated in any finite element parallel code while preserving the local structure of the algebraic system. Moreover, the analysis of the performance of these conditions in the *low* frequency regime, when using an On-Surface radiation condition formulation [12], revealed that these conditions are very accurate regardless of the slenderness of the boundary [4],[19]. In addition, it has been demonstrated that the *second-order* local DtN condition (DtN2) outperforms the widely-used second-order absorbing boundary conditions (BGT2) [5] when expressed in prolate spheroidal coordinates [17]-[18].

We propose to extend the investigation of the performance of the local approximate DtN2 absorbing boundary condition to the case of the *high* frequency regime. More specifically, we perform an analytical and numerical study to assess the effect of the slenderness of the exterior boundary on the accuracy and the efficiency of the proposed absorbing boundary condition. We conduct this study using a domain-based formulation, that is the artificial boundary is located at some distance from the surface of the scatterer, since the OSRC approach is not adapted for such an analysis, as previously observed in [2]. Note that similar approach has been adopted to study the performance of the BGT2 absorbing boundary condition in the case of circular-shaped scatterers [3],[8].

The remainder of this paper is as follows. In Section 2, we specify the nomenclature and assumptions, and formulate the considered three-dimensional

acoustic scattering problem in a bounded domain using the local approximate DtN2 absorbing boundary condition proposed in [4]. Section 3 is devoted to the analytical study of the mathematical properties of the solution of the resulting boundary value problem in the high frequency regime. The existence and the uniqueness of the solution are established. In addition, we assess the accuracy by analyzing the asymptotic behavior of the solution. Numerical results are also presented to illustrate the efficiency of the proposed absorbing boundary condition. Concluding remarks are presented in Section 3.

2 Preliminaries

2.1 Nomenclature and assumption

Throughout this paper, we use the prolate spheroidal coordinates (ξ, φ, θ) , related to the cartesian coordinates (x, y, z) by $x = b \sin \varphi \cos \theta$, $y = b \sin \varphi \sin \theta$, and $z = a \cos \varphi$, where $\varphi \in [0, \pi)$ and $\theta \in [0, 2\pi)$. The parameters a and b are the semi-major and the semi-minor axes respectively, and are given by $a = f \cosh \xi$ and $b = f \sinh \xi$ where ξ is strictly positive and the real number f is the interfocal distance ($f = \sqrt{a^2 - b^2}$). In addition, we adopt the following notations:

- k is a positive number representing the wavenumber.
- $R_{mn}^{(j)}(kf, \cosh \xi)$ is the radial spheroidal wave function of the j^{th} kind corresponding to the $(mn)^{\text{th}}$ (see p. 30 in [9]) where $(m, n) \in \mathbb{N}^2$ such that $n \geq m$.
- $S_{mn}(kf, \cos \varphi)$ is the angular spheroidal wave function corresponding to the $(mn)^{\text{th}}$ mode (see p. 16 in [9]).
- N_{mn} is the normalization factor associated to $S_{mn}(kf, \cos \varphi)$. N_{mn} is given by (see Eq. (3.1.32) p. 22 in [9]):

$$N_{mn} = \int_{-1}^1 [S_{mn}(kf, v)]^2 dv \quad (1)$$

- λ_{mn} is the prolate spheroidal eigenvalue (see p. 11 in [9]).
- Ω is a prolate spheroidal-shaped scatterer whose surface is denoted by Γ . Ω^c is the open complement in \mathbb{R}^3 of the domain $\bar{\Omega}$.
- a_Γ (resp. b_Γ) represents the semi-major (resp. semi-minor) axis of the scatterer Ω . e_Γ is the eccentricity
- Σ is an artificial boundary surrounding the scatterer Ω . Σ is assumed to be a prolate-spheroid surface.
- a_Σ (resp. b_Σ) is the semi-major (resp. semi-minor) axis of the prolate spheroidal-shaped domain whose surface is Σ . e_Σ is its eccentricity.
- Ω^b is a bounded computational domain whose interior (resp. exterior) boundary is Γ (resp. Σ).

- λ_{mn} are the prolate spheroidal eigenvalues (see p. 16 in [9]).
- Δ_Σ is the Laplace Beltrami operator on Σ .
- For a function F_{mn} , we denote its restriction on Γ by:

$$F_{mn|_\Gamma} = F_{mn}(e_\Gamma k a_\Gamma, e_\Gamma^{-1}) \quad (2)$$

Similarly, the restriction of F_{mn} on Σ is denoted by:

$$F_{mn|_\Sigma} = F_{mn}(e_\Sigma k a_\Sigma, e_\Sigma^{-1}) \quad (3)$$

- The partial derivative of the radial spheroidal wave function $R_{mn}^{(j)}$ with respect to the variable ξ is denoted by $R_{mn}^{(j)'}$, i.e.

$$R_{mn}^{(j)'} = \frac{\partial R_{mn}^{(j)}}{\partial \xi}; \quad j \in \mathbb{N} \quad (4)$$

- $r_{mn|_\Sigma}$ are complex numbers given by:

$$r_{mn|_\Sigma} = \frac{R_{mn|_\Sigma}^{(3)'}}{R_{mn|_\Sigma}^{(3)}} \quad (5)$$

- $r_{mn|_\Sigma}^{(j)}$ are complex numbers given by:

$$r_{mn|_\Sigma}^{(j)} = \begin{cases} \frac{R_{mn|_\Sigma}^{(3)'}}{R_{mn|_\Sigma}^{(3)}} & \text{if } j = 3 \\ \frac{R_{mn|_\Sigma}^{(4)'}}{R_{mn|_\Sigma}^{(4)}} & \text{if } j = 4 \end{cases} \quad (6)$$

Note that it follows from (5) and (6) that $r_{mn|_\Sigma}^{(3)} = r_{mn|_\Sigma}$

- $\|\cdot\|_2$ is the euclidean norm.

2.2 The acoustic scattering problem

Recall that the direct acoustic scattering problem by a sound-soft scatterer Ω can be formulated as follows [7]:

$$\begin{cases} \Delta u^{\text{scat}} + k^2 u^{\text{scat}} = 0 & \text{in } \Omega^c \\ u^{\text{scat}} = -u^{\text{inc}} & \text{on } \Gamma \\ \lim_{\|x\|_2 \rightarrow +\infty} \|x\|_2 \left[\frac{\partial u^{\text{scat}}}{\partial \|x\|_2} - i k u^{\text{scat}} \right] = 0 \end{cases} \quad (7)$$

where Δ is the Laplace operator, u^{scat} is the scattered field, and u^{inc} is the incident plane wave. Note that u^{inc} can be expressed, in prolate spheroid coordinates, as an infinite series (see Eq.(84) p. 386 in [21]):

$$u^{\text{inc}} = \sum_{m=0}^{+\infty} \sum_{n=m}^{+\infty} d_{mn}^{\text{inc}} u_{mn}^{(1)}(kf, \cosh \xi, \cos \varphi) \quad (8)$$

where the mn^{th} Fourier mode $u_{mn}^{(j)}$ is given by:

$$u_{mn}^{(j)}(kf, \cosh \xi, \cos \varphi) = R_{mn}^{(j)}(kf, \cosh \xi) \frac{S_{mn}(kf, \cos \varphi)}{\sqrt{N_{mn}}} \cos m\theta, \text{ for } j \in \mathbb{N}. \quad (9)$$

and the mn^{th} Fourier coefficient d_{mn}^{inc} is given by:

$$d_{mn}^{\text{inc}} = 2\varepsilon_m \frac{i^n}{\sqrt{N_{mn}}} S_{mn}(kf, \cos \varphi_0) \quad (10)$$

φ_0 is the incident angle of the plane wave u^{inc} , $\varepsilon_m = (2 - \delta_{0m})$, and δ_{0m} is the Kronecker symbol.

Furthermore, the solution u^{scat} of the exterior boundary value problem (7) can be expressed as an infinite series (see Eq. (11.36) p. 422 in [6]):

$$u^{\text{scat}} = \sum_{m=0}^{+\infty} \sum_{n=m}^{+\infty} d_{mn}^{\text{scat}} u_{mn}^{(3)}(kf, \cosh \xi, \cos \varphi) \quad (11)$$

where the mn^{th} Fourier outgoing mode $u_{mn}^{(3)}(kf, \cosh \xi, \cos \varphi)$ is given by Eq. (9), whereas the mn^{th} Fourier coefficient d_{mn}^{scat} is given by:

$$d_{mn}^{\text{scat}} = -2\varepsilon_m \frac{i^n}{\sqrt{N_{mn}}} \frac{R_{mn|_{\Gamma}}^{(1)}}{R_{mn|_{\Gamma}}^{(3)}} S_{mn}(e_{\Gamma}ka_{\Gamma}, \cos \varphi_0) \quad (12)$$

Observe that it follows from substituting Eq.(10) into Eq.(12) that:

$$d_{mn}^{\text{scat}} = - \frac{R_{mn|_{\Gamma}}^{(1)}}{R_{mn|_{\Gamma}}^{(3)}} d_{mn|_{\Gamma}}^{\text{inc}} \quad (13)$$

Note that the Dirichlet boundary condition, characterizing sound-soft scatterers, is used in the boundary value problem (7) for simplicity only. Analytical expressions for other boundary conditions can be also derived [6].

2.3 Bounded domain-based formulation

The application of finite element techniques when solving numerically the exterior boundary value problem (7) requires first to set it in a bounded domain. This is achieved, in the nonreflecting boundary conditions context, by surrounding the scatterer Ω with an artificial boundary Σ and prescribing a so-called absorbing boundary condition. Consequently, when setting on Σ the second-order local approximate DtN boundary condition suggested in [4], the exterior

acoustic scattering problem (7) is reformulated in the bounded domain Ω^b as follows:

$$\begin{cases} \Delta u^{\text{DtN}} + k^2 u^{\text{DtN}} = 0 & \text{in } \Omega^b \\ u^{\text{DtN}} = -u^{\text{inc}} & \text{on } \Gamma \\ \frac{\partial u^{\text{DtN}}}{\partial \mathbf{n}} = \frac{1}{a_\Sigma \sqrt{1 - e_\Sigma^2 \cos^2 \varphi}} T u^{\text{DtN}} & \text{on } \Sigma \end{cases} \quad (14)$$

where \mathbf{n} is the outward normal to the exterior boundary Σ and T is the second-order local approximate DtN operator expressed in prolate spheroid coordinates as follows [4]:

$$T u = \frac{\sqrt{1 - e_\Sigma^2}}{(\lambda_{01|\Sigma} - \lambda_{00|\Sigma}) e_\Sigma} \left\{ \left[\lambda_{01|\Sigma} r_{01|\Sigma} - \lambda_{00|\Sigma} r_{00|\Sigma} - \left(r_{00|\Sigma} - r_{01|\Sigma} \right) (e_\Sigma k a_\Sigma)^2 \cos^2 \varphi \right] u - \left(r_{00|\Sigma} - r_{01|\Sigma} \right) \Delta_\Sigma u \right\} \quad (15)$$

Note that the field u^{DtN} is an *approximation* of the scattered field u^{scat} . The goal of this study is to assess the accuracy of such an approximation and to provide practical guidelines for avoiding excessive computations when employing the boundary condition (15) for solving high frequency acoustic scattering problems.

3 Analytical study

We analyze the mathematical properties of the solution of the boundary value problem (14) in the high frequency regime. We also assess the efficiency of the second-order local approximate DtN boundary condition given by Eq. (15). Numerical results are presented for illustration.

3.1 Existence and uniqueness of the approximate solution

We investigate in this section the well-posedness nature of the boundary value problem (14). We state a necessary and sufficient condition to ensure the existence and the uniqueness of the solution u^{DtN} , and illustrate numerically this study.

3.1.1 Mathematical results

The approximate scattered field u^{DtN} can be expressed as an infinite series of outgoing modes $R_{mn}^{(3)}(kf, \cosh \xi)$ and incoming modes $R_{mn}^{(4)}(kf, \cosh \xi)$. More specifically, we have (see Eq. (16) p. 233 in [16]):

$$u^{\text{DtN}} = \sum_{m=0}^{+\infty} \sum_{n=m}^{+\infty} \left[d_{mn}^{\text{DtN}} u_{mn}^{(3)}(kf, \cosh \xi, \cos \varphi) + \tau_{mn}^{\text{DtN}} u_{mn}^{(4)}(kf, \cosh \xi, \cos \varphi) \right] \quad (16)$$

where $u_{mn}^{(j)}(kf, \cosh \xi, \cos \varphi)$ are given by Eq. (9).

The incoming waves are the reflections of the scattered field due to the presence of the artificial exterior boundary Σ . Note that in the case of a perfectly nonreflecting boundary condition, the Fourier coefficients must satisfy $\tau_{mn}^{\text{DtN}} = 0$ and $d_{mn}^{\text{DtN}} = d_{mn}^{\text{scat}}$ for all $(m, n) \in \mathbb{N}^2$ such that $n \geq m$. Therefore, the degree of transparency of any absorbing boundary condition, and thus the level of accuracy in the approximation as well as the computational cost, depend on (a) the magnitude of the reflection coefficients $|\tau_{mn}^{\text{DtN}}|$ of the incoming waves, and (b) the magnitude of the difference $|d_{mn}^{\text{DtN}} - d_{mn}^{\text{scat}}|$. These two quantities become very small (resp. very large) as the intensity of the reflected waves at the boundary Σ are negligible (resp. very important).

Next, we investigate the properties of these coefficients. We first define, for all $(m, n) \in \mathbb{N}^2$ such that $n \geq m$, the following wronskian-like expression:

$$W_{mn}^{3,4}(\Gamma, \Sigma) = R_{mn|\Gamma}^{(3)} \Psi_{mn|\Sigma}^{(4)} - R_{mn|\Gamma}^{(4)} \Psi_{mn|\Sigma}^{(3)} \quad (17)$$

where

$$\Psi_{mn|\Sigma}^{(j)} = R_{mn|\Sigma}^{(j)} \left[c_{mn|\Sigma} + r_{mn|\Sigma}^{(j)} \right], \text{ for } j = 3, 4. \quad (18)$$

and

$$c_{mn|\Sigma} = \frac{r_{00|\Sigma} (\lambda_{01|\Sigma} - \lambda_{mn|\Sigma}) - r_{01|\Sigma} (\lambda_{00|\Sigma} - \lambda_{mn|\Sigma})}{\lambda_{00|\Sigma} - \lambda_{01|\Sigma}} \quad (19)$$

Observe that when $\Sigma \equiv \Gamma$, Eq. (62) is the standard wronskian between $R_{mn|\Gamma}^{(3)}$ and $R_{mn|\Gamma}^{(4)}$.

The following result pertains to the existence and uniqueness of the Fourier coefficients d_{mn}^{DtN} and τ_{mn}^{DtN} .

Theorem 3.1 *The approximate scattered field u^{DtN} , solution of the boundary value problem (14), exists and is unique if and only if*

$$W_{mn}^{3,4}(\Gamma, \Sigma) \neq 0 \quad \forall (m, n) \in \mathbb{N}^2, n \geq m \quad (20)$$

Moreover, if condition (20) is satisfied, then the Fourier coefficients d_{mn}^{DtN} and τ_{mn}^{DtN} are given by:

$$\begin{cases} d_{mn}^{\text{DtN}} = \frac{\Psi_{mn|\Sigma}^{(4)} R_{mn|\Gamma}^{(3)}}{W_{mn}^{3,4}(\Gamma, \Sigma)} d_{mn}^{\text{scat}} \\ \tau_{mn}^{\text{DtN}} = \frac{\Psi_{mn|\Sigma}^{(3)} R_{mn|\Gamma}^{(3)}}{W_{mn}^{3,4}(\Gamma, \Sigma)} d_{mn}^{\text{scat}} \end{cases} \quad (21)$$

Proof of Theorem 3.1. First, we substitute the Fourier series representations of both the approximate scattered field u^{DtN} given by Eq.(16) and the incident plane wave u^{inc} given by Eq.(8) into the boundary conditions of the boundary value problem (14). Consequently, for all $(m, n) \in \mathbb{N}^2$ such that $n \geq m$, we have:

$$\begin{cases} d_{mn}^{\text{DtN}} R_{mn|\Gamma}^{(3)} + \tau_{mn}^{\text{DtN}} R_{mn|\Gamma}^{(4)} = -d_{mn}^{\text{inc}} R_{mn|\Gamma}^{(1)} & \text{on } \Gamma \\ d_{mn}^{\text{DtN}} \Psi_{mn|\Sigma}^{(3)} + \tau_{mn}^{\text{DtN}} \Psi_{mn|\Sigma}^{(4)} = 0 & \text{on } \Sigma \end{cases} \quad (22)$$

The linear 2×2 system (59) is invertible if and only if the condition (20) and we have:

$$\begin{cases} d_{mn}^{\text{DtN}} = -\frac{d_{mn}^{\text{inc}} \Psi_{mn|\Sigma}^{(4)} R_{mn|\Gamma}^{(1)}}{W_{mn}^{3,4}(\Gamma, \Sigma)} \\ \tau_{mn}^{\text{DtN}} = \frac{d_{mn}^{\text{inc}} \Psi_{mn|\Sigma}^{(3)} R_{mn|\Gamma}^{(1)}}{W_{mn}^{3,4}(\Gamma, \Sigma)} \end{cases} \quad (23)$$

We then conclude the proof of Theorem 3.1 by substituting Eq. (13) into Eq. (23). \square

Remark 3.2 Note that using Eqs. (62)-(19) for $n = 0, 1$, leads to:

$$\Psi_{0n|\Sigma}^{(3)} = 0 \quad \text{and} \quad W_{0n}^{3,4}(\Gamma, \Sigma) = \Psi_{0n|\Sigma}^{(4)} R_{0n|\Gamma}^{(3)}$$

Consequently, it follows from Theorem 3.1 that the Fourier coefficients corresponding to the first two modes satisfy:

$$d_{0n}^{\text{DtN}} = d_{0n}^{\text{scat}} \quad \text{and} \quad \tau_{0n}^{\text{DtN}} = 0; \quad n = 0, 1 \quad (24)$$

Hence, Theorem 3.1 states that the first two modes in the infinite series given by Eq. (16) are the exact modes propagating towards the infinity and do not reflect at the artificial boundary Σ . This result is not surprising since the second-order local approximate DtN boundary condition given by Eq. (15) was constructed to be exact for the first two modes [4].

Next, we analyze the properties of the $W_{mn}^{3,4}(\Gamma, \Sigma)$ to determine when condition (20) is fulfilled. The result below describes the asymptotic behavior of $W_{mn}^{3,4}(\Gamma, \Sigma)$ as $ka_\Gamma \rightarrow \infty$.

Proposition 3.3 For all $(m, n) \in \mathbb{N}^2$ such that $n \geq m$, the wronskian-like function $W_{mn}^{3,4}(\Gamma, \Sigma)$ given by Eq.(62) satisfies:

$$W_{mn}^{3,4}(\Gamma, \Sigma) \sim -\frac{2ie_\Sigma}{ka_\Gamma} e^{ik(a_\Gamma - a_\Sigma)}; \quad \text{as } ka_\Gamma \rightarrow \infty \quad (25)$$

Proof of Proposition 3.3. First, we use Eqs.(62)-(19), and rewrite $W_{mn}^{3,4}(\Gamma, \Sigma)$ as follows:

$$\begin{aligned} W_{mn}^{3,4}(\Gamma, \Sigma) = & R_{mn|\Gamma}^{(3)} R_{mn|\Sigma}^{(4)} r_{mn|\Sigma}^{(4)} - R_{mn|\Gamma}^{(4)} R_{mn|\Sigma}^{(3)} r_{mn|\Sigma}^{(3)} \\ & + c_{mn} \left[R_{mn|\Gamma}^{(3)} R_{mn|\Sigma}^{(4)} - R_{mn|\Gamma}^{(4)} R_{mn|\Sigma}^{(3)} \right] \end{aligned} \quad (26)$$

Next, we analyze the asymptotic behavior of each term in Eq. (26). Observe that when $ka_\Gamma \rightarrow \infty$ then necessarily $ka_\Sigma \rightarrow \infty$.

We have (see Eqs. (21.9.4)-(21.9.5) p. 756 in [1]):

$$R_{mn|\bullet}^{(3)} \sim \overline{R_{mn|\bullet}^{(4)}} \sim \frac{1}{ka_\bullet} e^{i(ka_\bullet - \frac{1}{2}(n+1)\pi)}; \quad ka_\bullet \rightarrow +\infty \quad (27)$$

where the symbole \bullet can be either Γ or Σ and the overline denotes the complex conjugate.

From Eq. (6) and Eq. 4.1.16, p. 32 in [9] (or Eq. 80 p. 3647 in [17]), we deduce that for $j = 3, 4$:

$$r_{mn|_\Sigma}^{(j)} \sim e_\Sigma k a_\Sigma \frac{h_n^{(j-2)'}(ka_\Sigma)}{h_n^{(j-2)}(ka_\Sigma)} ; \quad ka_\Sigma \rightarrow +\infty \quad (28)$$

where $h_n^{(1)}$ (resp. $h_n^{(2)}$) are the *spherical* Hankel functions of the first (resp. second) kind of order n [1].

On the other hand (see Eq. 10. 1.1 p. 437 [1]), we have

$$\frac{h_n^{(j-2)'}(z)}{h_n^{(j-2)}(z)} = \frac{H_{n+1/2}^{(j-2)'}(z)}{H_{n+1/2}^{(j-2)}(z)} - \frac{1}{2z} ; \quad j = 3, 4 \quad (29)$$

where $H_n^{(1)}$ (resp. $H_n^{(2)}$) are the Hankel functions of the first (resp. second) kind of order n [1].

Then, using the asymptotic behavior of the Hankel functions (see [1]), it follows from Eq.(28) and Eq.(29) that:

$$r_{mn|_\Sigma}^{(3)} \sim \overline{r_{mn|_\Sigma}^{(4)}} \sim e_\Sigma k a_\Sigma \left[i - \frac{1}{ka_\Sigma} - i \frac{n(n+1)}{2} \frac{1}{(ka_\Sigma)^2} \right] ; \quad ka_\Sigma \rightarrow +\infty \quad (30)$$

Consequently, it follows from Eqs.(26)-Eq.(27) and Eq.(30) that:

$$W_{mn}^{3,4}(\Gamma, \Sigma) \sim 2i \left[\Im(R_{mn|_\Gamma}^{(3)} \overline{R_{mn|_\Sigma}^{(3)} r_{mn|_\Sigma}^{(3)}}) + c_{mn} \Im(R_{mn|_\Gamma}^{(3)} \overline{R_{mn|_\Sigma}^{(3)}}) \right] ; \quad ka_\Gamma \rightarrow +\infty \quad (31)$$

Next, we derive the asymptotic behavior of the coefficients c_{mn} given by Eq.(19) as $ka_\Sigma \rightarrow +\infty$. To do this, we first recall the asymptotic behavior of the prolate spheroidal eigenvalues $\lambda_{mn|_\Sigma}$ as $ka_\Sigma \rightarrow +\infty$ (see Eq. 21.7.6 p. 754 in [1]):

$$\lambda_{mn|_\Sigma} \sim (2n - 2m + 1) e_\Sigma k a_\Sigma ; \quad ka_\Sigma \rightarrow +\infty \quad (32)$$

Hence, applying the asymptotic behavior given by Eq.(32) together with the asymptotic behavior of $r_{mn|_\Sigma}^{(3)}$ for $(m, n) = (0, 0), (0, 1)$ (see Eq. (30)), we deduce that:

$$c_{mn|_\Sigma} \sim -e_\Sigma k a_\Sigma \left[i - \frac{1}{ka_\Sigma} + i(m-n) \frac{1}{(ka_\Sigma)^2} \right] ; \quad ka_\Sigma \rightarrow +\infty \quad (33)$$

Finally, (25) results from substituting Eq.(27), Eq.(30), and Eq.(33) into Eq.(31). This concludes the proof of Proposition 3.3.

□

Proposition 3.3 states that $|W_{mn}^{3,4}(\Gamma, \Sigma)| \sim \frac{2e_\Sigma}{ka_\Gamma} \neq 0$ as $ka_\Gamma \rightarrow \infty$. Consequently, it follows from Theorem 3.1 the following existence and uniqueness result in the high frequency regime:

Corollary 3.4 *The solution of the boundary value problem (14) exists and is unique for large values of ka_Γ .*

Remark 3.5 *The result stated in Corollary 3.4 proves that the Fourier coefficients d_{mn}^{DtN} and τ_{mn}^{DtN} always exist and are unique in the high frequency regime regardless of the location of the exterior boundary Σ with respect to Γ . This remark shows that the position of the exterior boundary Σ is important for the accuracy only.*

The next result addresses the particular case of the first two modes since the proposed absorbing boundary condition is, by construction, exact when applied to them [4].

Proposition 3.6 *The necessary and sufficient condition given by Eq.(20) is always satisfied for the first two modes. Furthermore, we have:*

$$W_{0n}^{3,4}(\Gamma, \Sigma) = \frac{R_{0n\Gamma}^{(3)}}{R_{0n\Sigma}^{(3)}} \frac{-2i}{e_\Sigma ka_\Sigma (e_\Sigma^{-2} - 1)} ; \quad \text{for } n = 0, 1 \quad (34)$$

Proof of Proposition 3.6. First, we use Eq.(5) to rewrite the expression of the coefficients $c_{0n|\Sigma}$ ($n = 0, 1$) given by Eq. (19) as follows:

$$c_{0n|\Sigma} = -r_{0n|\Sigma} = -\frac{R_{0n|\Sigma}^{(3)'}}{R_{0n|\Sigma}^{(3)}} ; \quad \text{for } n = 0, 1 \quad (35)$$

Then, for $n = 0, 1$, we substitute Eq.(6) and Eq.(35) into Eq.(26) and obtain:

$$W_{0n}^{3,4}(\Gamma, \Sigma) = R_{0n|\Gamma}^{(3)} R_{0n|\Sigma}^{(4)'} - R_{0n|\Gamma}^{(4)} R_{0n|\Sigma}^{(3)'} - \frac{R_{0n|\Sigma}^{(3)'}}{R_{0n|\Sigma}^{(3)}} \left[R_{0n|\Gamma}^{(3)} R_{0n|\Sigma}^{(4)} - R_{0n|\Gamma}^{(4)} R_{0n|\Sigma}^{(3)} \right]$$

Thus,

$$W_{0n}^{3,4}(\Gamma, \Sigma) = \frac{R_{0n|\Gamma}^{(3)}}{R_{0n|\Sigma}^{(3)}} W_{0n}^{3,4}(\Sigma) ; \quad n = 0, 1 \quad (36)$$

where $W_{0n}^{3,4}(\Sigma)$ is the wronskien between $R_{0n|\Gamma}^{(3)}$ and $R_{0n|\Gamma}^{(4)}$, that is:

$$W_{0n}^{3,4}(\Sigma) = R_{0n|\Sigma}^{(3)} R_{0n|\Sigma}^{(4)'} - R_{0n|\Sigma}^{(4)} R_{0n|\Sigma}^{(3)'} ; \quad n = 0, 1$$

which can be rewritten, using the representation of $R_{0n|\Sigma}^{(j)}$ ($j = 3, 4$) in terms of $R_{0n|\Sigma}^{(l)}$ ($l = 1, 2$)(see Eq. 4.1.18, p. 32 in [9]), as follows:

$$W_{0n}^{3,4}(\Sigma) = -2i W_{0n}^{1,2}(\Sigma) ; \quad n = 0, 1 \quad (37)$$

Moreover, we have (see Eq. 4.1.21, p. 32 in [9] or Appendix C in [19]):

$$W_{mn}^{1,2}(\Sigma) = \frac{1}{e_\Sigma ka_\Sigma (e_\Sigma^{-2} - 1)} ; \quad \forall (m, n) \in \mathbb{N}^2 \quad \text{and } n \geq m \quad (38)$$

Eq.(34) is then an immediate consequence of substituting Eq.(37) and Eq.(38) into Eq.(36).

□

Remark 3.7 *The result stated in Proposition 3.6 proves that the Fourier coefficients d_{mn}^{DtN} and r_{mn}^{DtN} corresponding to the first two modes, i. e. $(m, n) = (0, 0), (0, 1)$ exist and are unique independently of both the frequency regime and the position of the artificial boundary Σ . This property along with the observation made in Remark 3.2 allow to conclude, as expected, that Eq. (24) always holds.*

3.1.2 Illustrative numerical results

Proposition 3.3 proves that the necessary and sufficient condition (20) in Theorem 3.1 is satisfied for all modes but in the high frequency regime only, whereas Proposition 3.6 states that, in the case of the first two modes, this condition holds in all frequency band. Note that these two results are valid with no restriction on the location of the artificial boundary Σ with respect to the boundary Γ of the scatterer Ω .

We have investigated numerically the validity of condition (20) [19]. More specifically, we have assumed that the semi-major and semi-minor axes satisfy respectively $a_\Sigma = \sigma a_\Gamma$ and $b_\Sigma = \sigma b_\Gamma$. The positive real number σ , called the *widening coefficient*, satisfies $\sigma > 1$. Such an assumption implies that the two boundaries have the same eccentricity ($e_\Sigma = e_\Gamma = e$). Note that $\sigma = 1$ corresponds to the extreme case scenario where $\Sigma \equiv \Gamma$, the OSRC formulation [12], [4]. We have analyzed the dependence of $|W_{mn}^{3,4}(\Gamma, \Sigma)|$ with respect to the widening parameter σ . The obtained results [19] tend to indicate that condition (20) holds for all modes and values of ka_Γ with no restriction on the position of Σ . For illustration purpose, we present in Figs.(1)-(2) two sets of results obtained for two frequency values $ka = 10$ and 20 , and "very" elongated boundaries $e_\Sigma = e_\Gamma = 0.9$. The results depicted in Figs. (1)-(2) correspond six different modes ranging from the lowest mode $(m, n) = (0, 0)$ to a higher mode corresponding to $(m, n) = (7, 7)$. The following observations are noteworthy:

- The necessary and sufficient condition (20) is clearly satisfied.
- These results suggest that the Wronskian-like function $|W_{mn}^{3,4}(\Gamma, \Sigma)|$ is an increasing function with respect to the widening parameter σ .
- The results depicted in Figs. (1)-(2), together with those reported in [19], suggest the following conjecture:

$$|W_{mn}^{3,4}(\Gamma, \Sigma)| \geq \frac{2}{e_\Gamma ka_\Gamma (e_\Gamma^{-2} - 1)} ; \quad \forall (m, n) \in \mathbb{N}^2 \quad \text{and} \quad n \geq m \quad (39)$$

Note that the lower bound of Eq.(39) corresponds to twice the value of $|W_{mn}^{1,2}(\Gamma)|$ (see Eq. (38)). This conjecture can be easily established in the case of the first two modes (see Eq. (34) in Proposition 3.6).

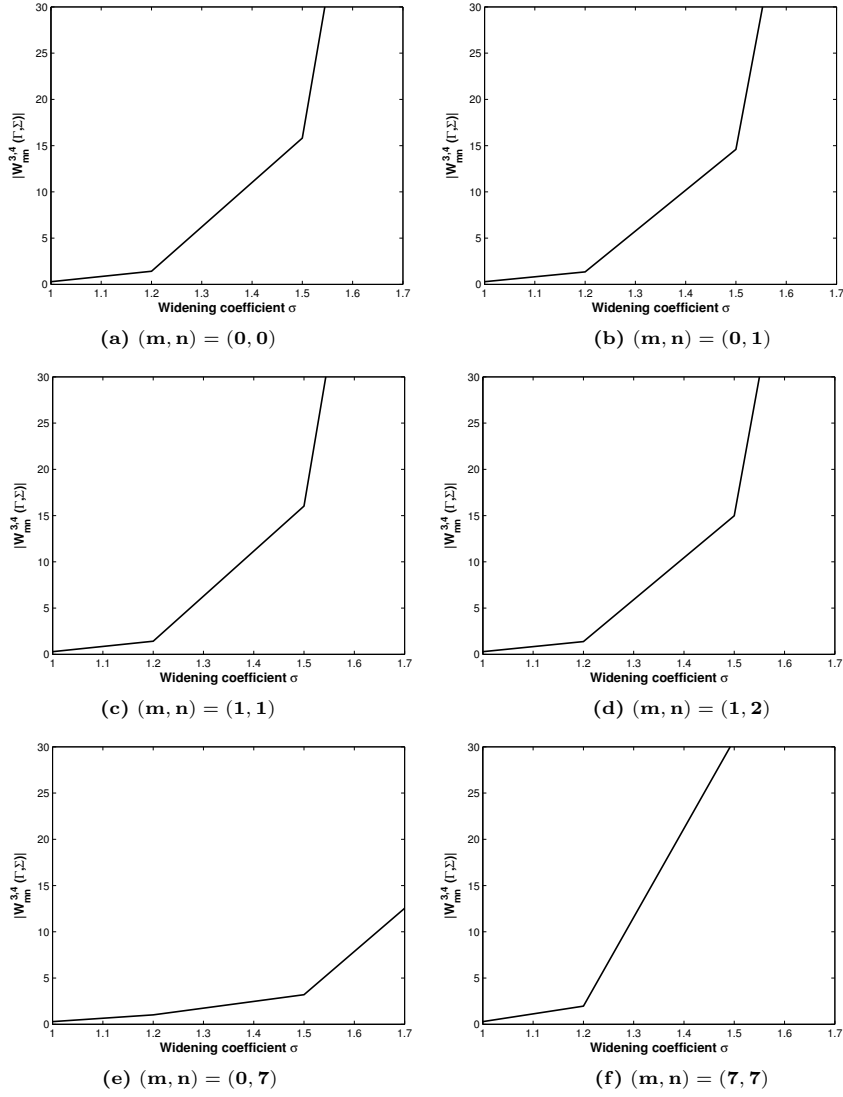


Figure 1: Sensitivity of the Wronskien-like function $|W_{mn}^{3,4}(\Gamma, \Sigma)|$ given by Eq.(62) to the widening coefficient $\sigma = \frac{a_\Sigma}{a_\Gamma}$. Case where $e_\Gamma = e_\Sigma = 0.9$ and $ka_\Gamma = 10$.

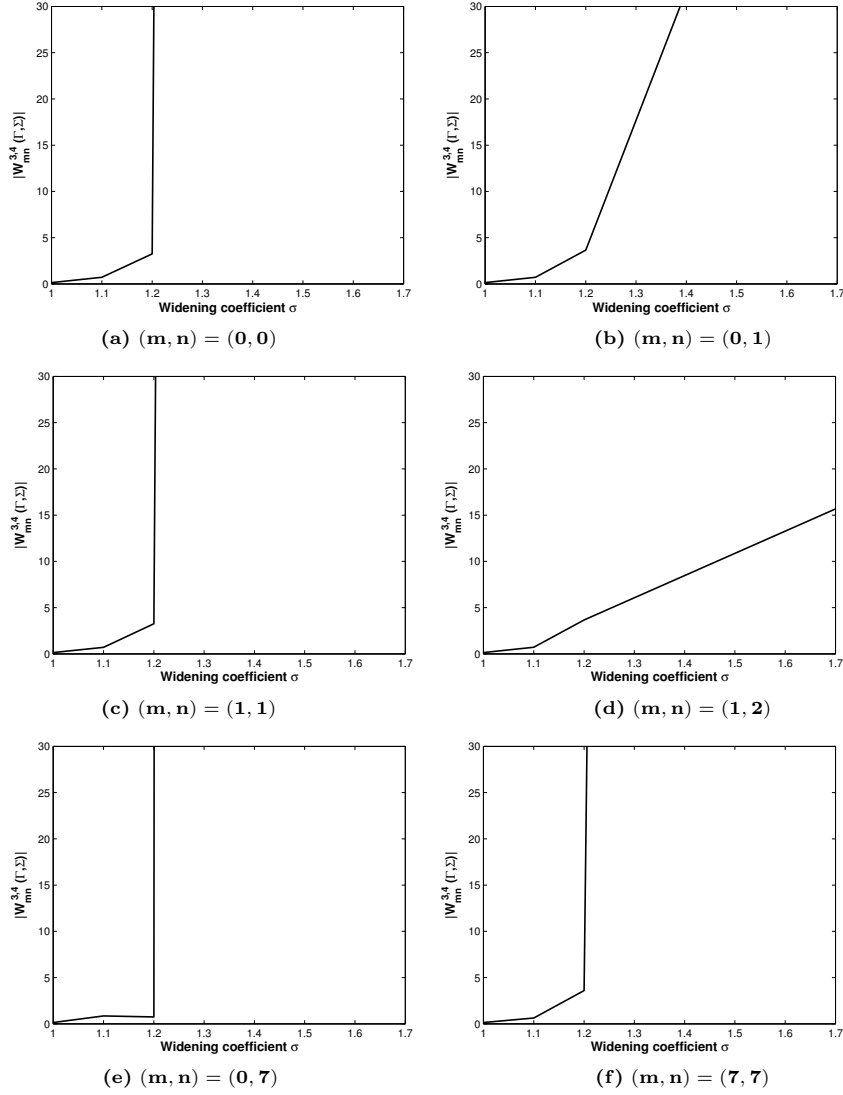


Figure 2: Sensitivity of the Wronskien-like function $|W_{mn}^{3,4}(\Gamma, \Sigma)|$ given by Eq.(62) to the widening coefficient $\sigma = \frac{a_\Sigma}{a_\Gamma}$. Case where $e_\Gamma = e_\Sigma = 0.9$ and $ka_\Gamma = 20$.

3.2 Accuracy of the approximate scattered field

Next, we assess the accuracy performance of the proposed approximate boundary condition in the high frequency regime. First, we perform an analytical study, and then we present numerical results to illustrate the potential of the proposed local approximate DtN2 absorbing boundary condition for solving accurately acoustic scattering problems.

3.2.1 Mathematical results

We compare the approximate scattered field u^{DtN} given by Eq. (16) to the exact scattered field u^{scat} given by Eq. (11) by analyzing the asymptotic behavior of the Fourier coefficients given by Eq. (21) as $ka_\Gamma \rightarrow \infty$. The following result analyzes the asymptotic behavior of the propagating Fourier coefficients corresponding to the approximate scattered field u^{scat} given by Eq. (11). Recall that the first two modes in the infinite series given by Eq. (16) are the exact modes propagating towards the infinity and do not reflect at the artificial boundary Σ (see Eq. (24)). Therefore, the following analysis addresses the case of the remaining modes. To do this, we introduce the following set

$$\mathcal{N} = \{(m, n) \in \mathbb{N}^2 \setminus \{(0, 0), (0, 1)\} \text{ such that } n \geq m\} \quad (40)$$

Proposition 3.8 *For all $(m, n) \in \mathcal{N}$, the propagating Fourier coefficients d_{mn}^{DtN} given by Eq.(21) satisfy:*

$$d_{mn}^{\text{DtN}} \sim d_{mn}^{\text{scat}} ; \quad \text{as } ka_\Gamma \rightarrow \infty \quad (41)$$

where d_{mn}^{scat} are the Fourier coefficients corresponding to the exact scattered field u^{scat} (see Eqs. (11)-(12)).

Proof of Proposition 3.8. In order to obtain the asymptotic behavior of the Fourier coefficients d_{mn}^{DtN} given by Eq. (21), we first derive the asymptotic behavior of the numerator $\Psi_{mn|\Sigma}^{(4)} R_{mn|\Gamma}^{(3)}$ where $\Psi_{mn|\Sigma}^{(4)}$ is given by Eq. (18). To do this, we substitute into Eq. (18) the asymptotic behavior of (a) $R_{mn|\Sigma}^{(4)}$ given by Eq. (27), (b) $r_{mn|\Sigma}^{(4)}$ given by Eq. (30), and (c) $c_{mn|\Sigma}$ given by Eq. (33). Then, as $ka_\Gamma \rightarrow \infty$, we obtain:

$$\Psi_{mn|\Sigma}^{(4)} R_{mn|\Gamma}^{(3)} \sim \frac{1}{ka_\Gamma ka_\Sigma} e^{ik(a_\Gamma - a_\Sigma)} \left[-e_\Sigma ka_\Sigma \left(i - \frac{1}{ka_\Sigma} \right) + e_\Sigma ka_\Sigma \left(-i - \frac{1}{ka_\Sigma} \right) \right] \quad (42)$$

Proposition 3.8 is then an immediate consequence of substituting Eq. (25) (see Proposition 3.3) and Eq. (42) into Eq. (21).

□

Remark 3.9 *Proposition 3.8 indicates that $\frac{\tau_{mn}^{\text{DtN}}}{d_{mn}^{\text{scat}}} \rightarrow 0$ as $ka_\Gamma \rightarrow \infty$. This suggests that, for large values of the wavenumber ka_Γ , the propagating term of the approximate scattered field u^{DtN} (see Eq. (11)) becomes a good approximation the exact scattered field u^{scat} .*

Next, we analyze the asymptotic behavior of the reflection Fourier coefficients τ_{mn}^{DtN} given by Eq. (21). The following result compares asymptotically τ_{mn}^{DtN} to the Fourier coefficients d_{mn}^{scat} corresponding to the exact scattered field u^{scat} .

Proposition 3.10 *For all $(m, n) \in \mathcal{N}$, the reflection Fourier coefficients τ_{mn}^{DtN} given by Eq.(21) satisfy:*

$$\tau_{mn}^{\text{DtN}} \sim \frac{(-1)^{n+1}}{2(ka_\Sigma)^2} \left(m - n + \frac{n(n+1)}{2} \right) e^{2ika_\Sigma} d_{mn}^{\text{scat}} ; \quad \text{as } ka_\Gamma \rightarrow \infty \quad (43)$$

where d_{mn}^{scat} are the Fourier coefficients corresponding to the exact scattered field u^{scat} (see Eqs. (11)-(12)).

Proof of Proposition 3.10. In order to obtain the asymptotic behavior of the Fourier coefficients τ_{mn}^{DtN} given by Eq. (21), we first derive the asymptotic behavior of the numerator $\Psi_{mn|\Sigma}^{(3)} R_{mn|\Gamma}^{(3)}$ where $\Psi_{mn|\Sigma}^{(3)}$ is given by Eq. (18). To do this, we substitute into we substitute into Eq. (18) the asymptotic behavior of (a) $R_{mn|\Sigma}^{(3)}$ given by Eq. (27), (b) $r_{mn|\Sigma}^{(3)}$ given by Eq. (30), and (c) $c_{mn|\Sigma}$ given by Eq. (33). Then, we obtain:

$$\Psi_{mn|\Sigma}^{(3)} R_{mn|\Gamma}^{(3)} \sim \frac{-ie_\Sigma}{ka_\Gamma(ka_\Sigma)^2} \left(m - n + \frac{n(n+1)}{2} \right) e^{i(k(a_\Gamma+a_\Sigma)-(n+1)\pi)} ; \quad \text{as } ka_\Gamma \rightarrow \infty \quad (44)$$

Next, we substitute (25) (see Proposition 3.3) and Eq. (44) into Eq. (21). The, we obtain:

$$\tau_{mn}^{\text{DtN}} \sim \frac{1}{2(ka_\Sigma)^2} \left(m - n + \frac{n(n+1)}{2} \right) e^{2ika_\Sigma} e^{-i(n+1)\pi} d_{mn}^{\text{scat}} ; \quad \text{as } ka_\Gamma \rightarrow \infty \quad (45)$$

which concludes the proof of Proposition 3.10. \square

Remark 3.11 *Proposition 3.10 suggests that, for large values of the wavenumber ka_Γ , the reflected waves in the approximate scattered field u^{DtN} (see Eq. Eq. (11)) become smaller (decay to zero) compared to the (propagating) exact scattered field u^{scat} .*

The next result indicates the rate of decay of the reflection Fourier coefficients τ_{mn}^{DtN} as $ka_\Gamma \rightarrow \infty$.

Theorem 3.12 *For all $(m, n) \in \mathcal{N}$, the reflection Fourier coefficients τ_{mn}^{DtN} given by Eq.(21) satisfy:*

$$|\tau_{mn}^{\text{DtN}}| < \frac{2\kappa}{\pi^{1/4}} \left(\frac{n(n-1)}{2} + m \right) \left(\frac{e_\Gamma a_\Gamma}{a_\Sigma} \right)^{1/8} \frac{1}{(ka_\Sigma)^{15/8}} ; \quad \text{as } ka_\Gamma \rightarrow \infty \quad (46)$$

where the positive constant κ satisfies:

$$\kappa \approx 1.086435 \quad (47)$$

The proof of Theorem 3.12 is based on the following intermediate result that provides an upper bound on the Fourier coefficients corresponding to the incident plane wave u^{inc} given by Eq. (8).

Lemma 3.13 For all $(m, n) \in \mathcal{N}$, the Fourier coefficients d_{mn}^{inc} given by Eq. (10) satisfy:

$$|d_{mn|_{\Gamma}}^{\text{inc}}| < 4\kappa \left(\frac{\sqrt{e_{\Gamma} k a_{\Gamma}}}{\pi} \right)^{1/4}; \quad ka_{\Gamma} \rightarrow +\infty \quad (48)$$

where the positive constant κ is given by Eq. (47).

Proof of Lemma 3.13. Recall that, as $ka_{\Gamma} \rightarrow +\infty$, the asymptotic behavior of the angular spheroidal wave function corresponding to the $(mn)^{\text{th}}$ mode is given by (see Eq. (3.251) p. 243 in [15]):

$$\begin{aligned} S_{mn}(e_{\Gamma} k a_{\Gamma}, \cos \varphi_0) \sim & (-1)^m \left(\frac{4\sqrt{e_{\Gamma} k a_{\Gamma}}}{\pi} \right)^{1/4} \frac{1}{(n-m)!} \left(\frac{(n+m)!}{2n+1} \right)^{1/2} \\ & \cdot (1 - \cos^2 \varphi_0)^{m/2} D_{n-m} \left((2\sqrt{e_{\Gamma} k a_{\Gamma}})^{1/2} \cos \varphi_0 \right) \end{aligned} \quad (49)$$

where $D_{n-m} \left((2\sqrt{e_{\Gamma} k a_{\Gamma}})^{1/2} \cos \varphi \right)$ are the parabolic cylinder functions [1]. These functions can be expressed in terms of the Hermite polynomials as follows (see Eq. (19.3.1) p. 687 and Eq. (19.13.1) p. 691 in [1]):

$$\begin{aligned} D_{n-m} \left((2\sqrt{e_{\Gamma} k a_{\Gamma}})^{1/2} \cos \varphi_0 \right) = & 2^{(m-n)/2} H_{n-m} \left((e_{\Gamma} k a_{\Gamma})^{1/4} \cos \varphi_0 \right) \\ & \cdot \exp \left(-\frac{\sqrt{e_{\Gamma} k a_{\Gamma}} \cos^2 \varphi_0}{2} \right) \end{aligned} \quad (50)$$

Moreover, the Hermite polynomials satisfy (see Eq. (22.14.17) p. 786 in [1]):

$$\left| H_{n-m} \left((e_{\Gamma} k a_{\Gamma})^{1/4} \cos \varphi_0 \right) \right| < \kappa 2^{(n-m)/2} \sqrt{(n-m)!} \exp \left(\frac{\sqrt{e_{\Gamma} k a_{\Gamma}} \cos^2 \varphi_0}{2} \right) \quad (51)$$

In addition, we have (see Eq. 3.23 p. 237 in [15]) that:

$$N_{mn} = \frac{2}{2n+1} \frac{(n+m)!}{(n-m)!} \quad (52)$$

Therefore, Eq. (48) results from substituting Eqs. (49)-(52) into Eq. (10). \square

Proof of Theorem 3.12. It follows from Eq. (43) that

$$|\tau_{mn}^{\text{DtN}}| \sim \frac{1}{2(k a_{\Sigma})^2} \left(\frac{n(n-1)}{2} + m \right) |d_{mn}^{\text{scat}}|; \quad \text{as } ka_{\Gamma} \rightarrow \infty \quad (53)$$

On the other hand, we have (see Eq. (21.9.4) p. 756 in [1]):

$$R_{mn|_{\Gamma}}^{(1)} \sim \Re(R_{mn|_{\Gamma}}^{(3)}); \quad ka_{\Gamma} \rightarrow +\infty \quad (54)$$

where $\Re(z)$ designates the real part of the complex number z . Therefore, it follows from Eq. (13) and Eq. (54) that:

$$|d_{mn}^{\text{scat}}| \sim \left| \cos \left(ka_{\Gamma} - \frac{1}{2}(n+1)\pi \right) \right| |d_{mn|_{\Gamma}}^{\text{inc}}|; \quad ka_{\Gamma} \rightarrow +\infty \quad (55)$$

Eq. (46) results from substituting Eq. (48) and Eq. (55) into Eq. (53). \square

Remark 3.14 *Theorem 3.12 states that the reflection Fourier coefficients decay faster than $\frac{1}{(ka_{\Sigma})^{15/8}}$. This result along with Proposition 3.8 prove that, as $ka_{\Gamma} \rightarrow \infty$ u^{DtN} , the solution of the boundary value problem (14), tends to the exact scattered field u^{scat} , the solution of the acoustic scattering problem (7).*

3.2.2 Illustrative numerical results

We assess numerically the performance of the local approximate DtN2 boundary condition given by Eq. (15) when applied in domain-based formulation for solving acoustic scattering problems (14).

Similarly to the previous numerical investigation (see Section 3.1.2) we perform this numerical investigation in the particular case where the two boundaries Γ and Σ are parallel. Hence, we assume that the semi-major and semi-minor axes satisfy respectively $a_{\Sigma} = \sigma a_{\Gamma}$ and $b_{\Sigma} = \sigma b_{\Gamma}$. The positive real number σ , called the *widening* coefficient, satisfies $\sigma \geq 1$. Recall that such an assumption implies that the two boundaries have the same eccentricity, that is $e_{\Sigma} = e_{\Gamma} = e$. We analyze the sensitivity of the accuracy to the value of σ , that is the position of the exterior boundary Σ with respect to the boundary Γ of the prolate spheroidal-shaped scatterer Ω . This is achieved by computing the 2-norm of (a) the reflection Fourier coefficients τ_{mn}^{DtN} given by Eq. (21) as a function of the distance between the interior boundary Γ and the artificial boundary Σ , i.e.

$$\sigma \rightarrow \left(\sum_{m=0}^{+\infty} \sum_{n=m}^{+\infty} |\tau_{mn}^{\text{DtN}}|^2 \right)^{1/2}$$

and (b) the relative error between the approximate solution u^{DtN} given by Eq. (16) and the scattered field u^{scat} given by Eq. (11) as a function of σ , i.e.

$$\sigma \rightarrow \frac{\left(\sum_{m=0}^{+\infty} \sum_{n=m}^{+\infty} (|d_{mn}^{\text{app}} - d_{mn}^{\text{scat}}|^2 + |\tau_{mn}^{\text{app}}|^2) \right)^{1/2}}{\left(\sum_{m=0}^{+\infty} \sum_{n=m}^{+\infty} |d_{mn}^{\text{scat}}|^2 \right)^{1/2}}$$

The goal in part (a) is to measure the intensity of the reflected waves, and therefore to assess the level of transparency of the proposed boundary condition, whereas in part (b) we evaluate the accuracy as a function of the distance between the two boundaries. We compare the performance of this condition to

the performance of the so-called BGT2 boundary condition designed in spherical coordinates in [5] and expressed in prolate spheroid coordinates in [17]. Note that the expression of Fourier coefficients d_{mn}^{BGT2} and τ_{mn}^{BGT2} corresponding to BGT2 condition can be found in the Appendix (see Eq.(??)) . For illustration purpose, we present the results of two sets of numerical experiments performed where we have set $ka = 10$ and 20 . These results have been obtained for three eccentricity values $e_\Sigma = e_\Gamma = 0.1$ corresponding to a prolate spheroid "close" to a sphere, 0.4 corresponding to a "regular" prolate-spheroid boundary, and 0.9 corresponding to a "very" elongated regular prolate-spheroid boundary. The results depicted in Figs. (3)- (14) are obtained for three incident angles $\varphi_0 = 0$, $\frac{\pi}{4}$, and $\frac{\pi}{2}$. The following observation are noteworthy:

- Figs. (3)-(8) indicate that the proposed DtN2 boundary condition given by Eq. (15) produces "little" reflections, especially for large eccentricity values. More specifically, for large eccentricity values ($e = 0.9$), the 2-norm of the reflection coefficients is already below 1% as soon as $\sigma > 1.2$, which corresponds to a small computational domain Ω^b . This result illustrate the high level of transparency of the proposed DtN2 boundary condition when applied on very elongated boundaries. On the other hand, for small eccentricity values corresponding to boundaries close to sphere ($e = 0.1$), the 2-norm of the reflection coefficients remains of order 5% for all frequencies even when the exterior boundary Σ is placed very far from the boundary Γ of the scatterer Ω , i.e. for large values of σ .
- The results depicted Figs. (9)-(14) indicate that proposed DtN2 boundary condition delivers the solution with a high level of accuracy. Indeed, for large eccentricity values ($e = 0.9$), the relative error, in the 2-norm sense, is below .1% as soon as $\sigma > 1.2$, which corresponds to a small computational domain Ω^b . This observation suggests that the proposed DtN2 boundary condition is very efficient when applied on very elongated boundaries. Observe that, for small eccentricity values ($e = 0.1$), the DtN2 boundary condition retains a good level of accuracy, the relative error is of order 1% when $\sigma > 1.4$ which corresponds to a relatively small computational domain.
- Figs. (3)-(14) show that the proposed DtN2 boundary condition given by Eq. (15) outperforms the BGT2 boundary condition when expressed in prolate spheroid coordinates in [17]. This superiority is more noticeable for small eccentricity values which is surprising because when $e \rightarrow 0$ both conditions tend to the same boundary condition.

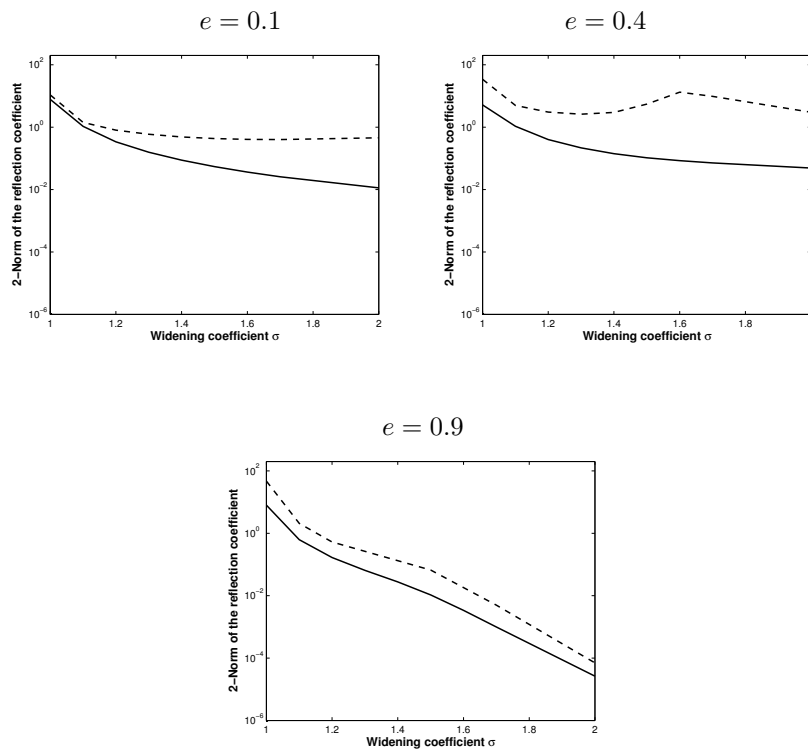


Figure 3: Sensitivity of the reflection coefficients to the widening parameter σ for $ka = 10$ and incident angle $\varphi_0 = 0$; DtN2 (plain), BGT2 (dashed).

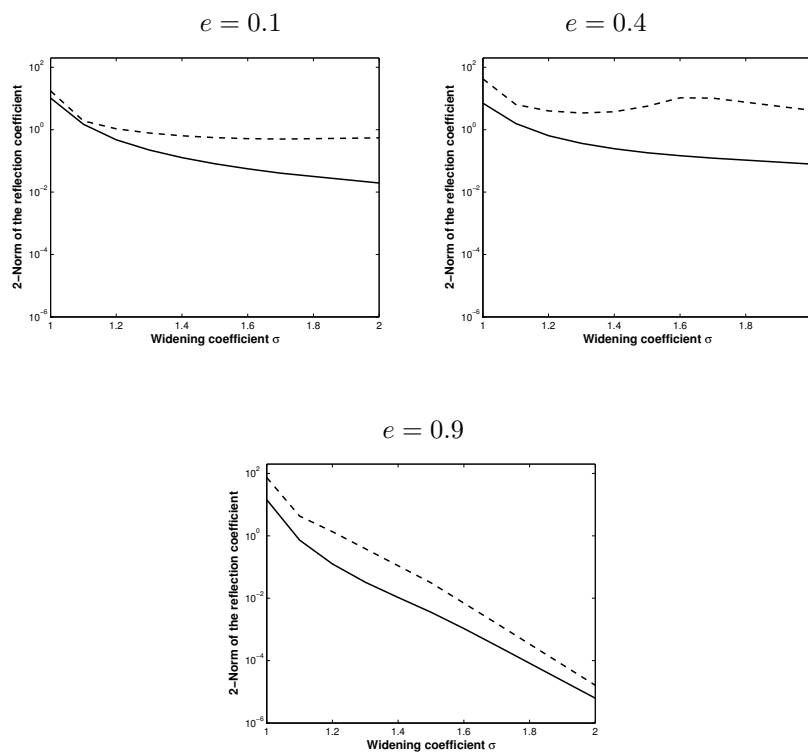


Figure 4: Sensitivity of the reflection coefficients to the widening parameter σ for $ka = 10$ and incident angle $\varphi_0 = \frac{\pi}{4}$; DtN2 (plain), BGT2 (dashed).

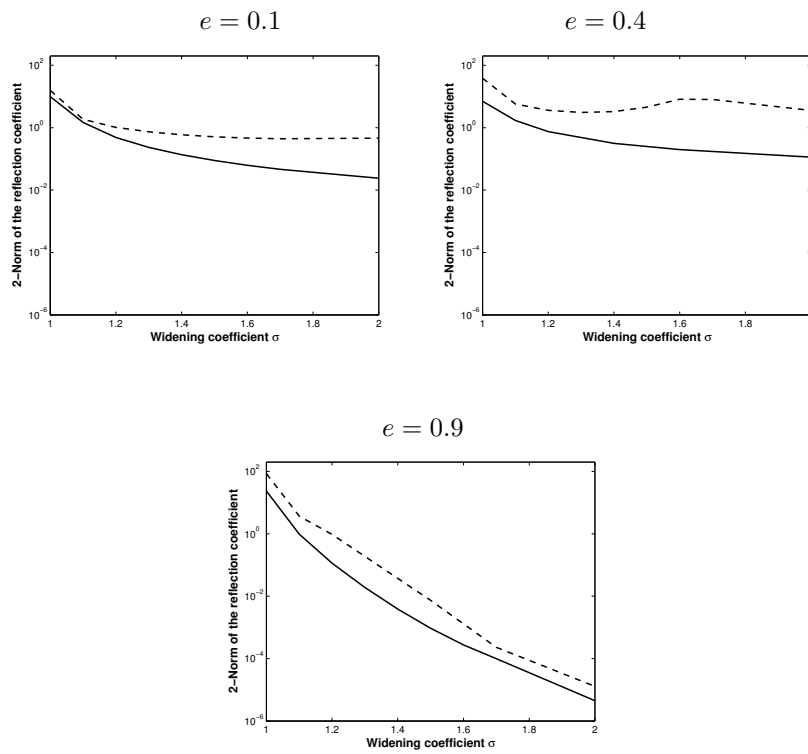


Figure 5: Sensitivity of the reflection coefficients to the widening parameter σ for $ka = 10$ and incident angle $\varphi_0 = \frac{\pi}{2}$; DtN2 (plain), BGT2 (dashed).

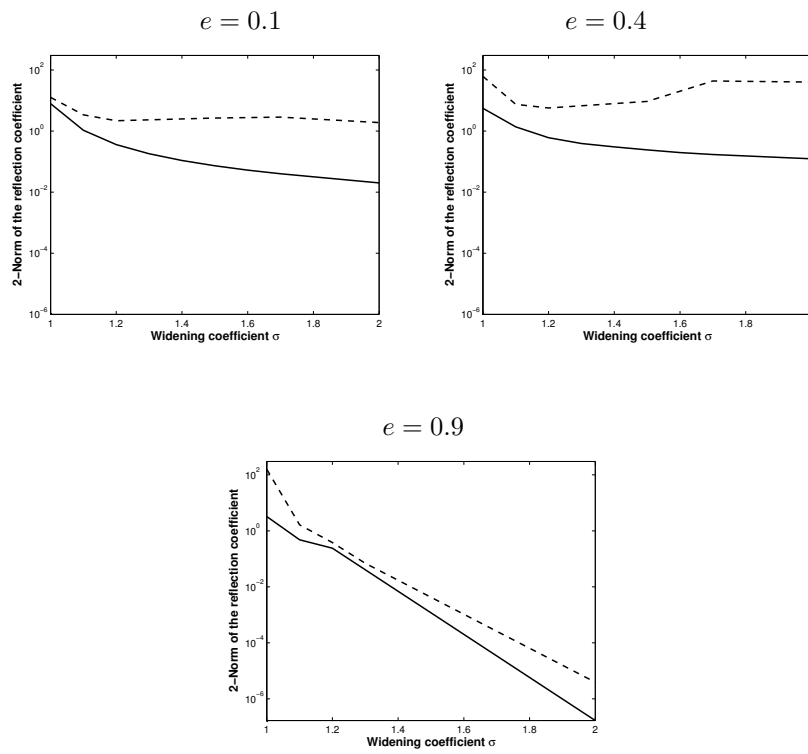


Figure 6: Sensitivity of the reflection coefficients to the widening parameter σ for $ka = 20$ and incident angle $\varphi_0 = 0$; DtN2 (plain), BGT2 (dashed).

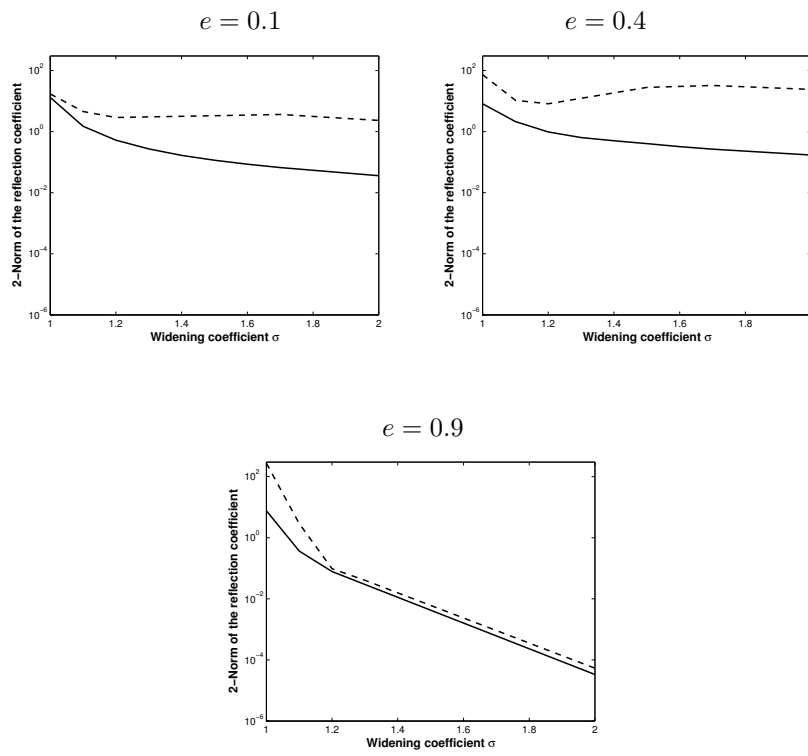


Figure 7: Sensitivity of the reflection coefficients to the widening parameter σ for $ka = 20$ and incident angle $\varphi_0 = \frac{\pi}{4}$; DtN2 (plain), BGT2 (dashed).

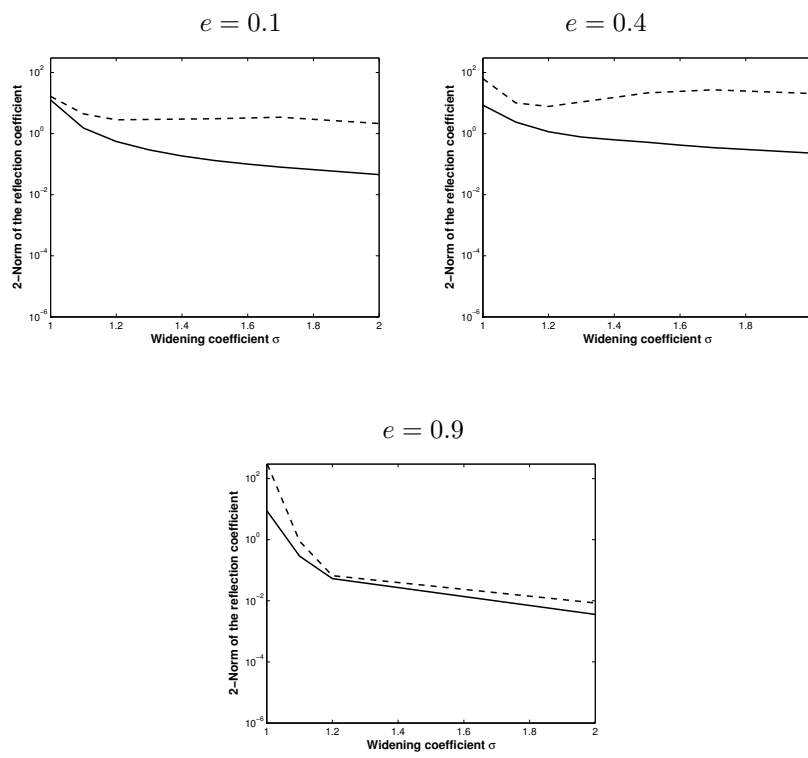


Figure 8: Sensitivity of the reflection coefficients to the widening parameter σ for $ka = 20$ and incident angle $\varphi_0 = \frac{\pi}{2}$; DtN2 (plain), BGT2 (dashed).

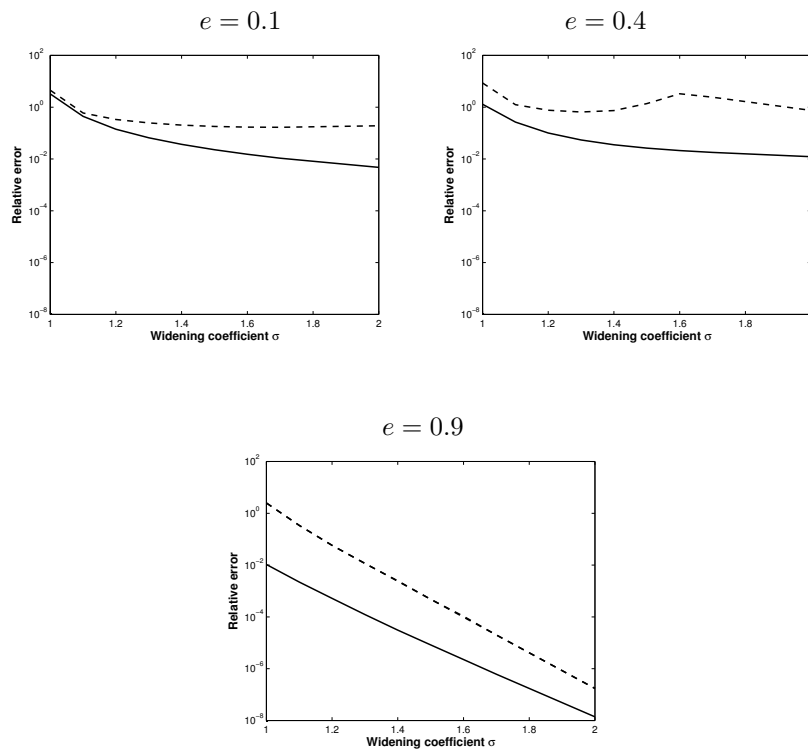


Figure 9: Sensitivity of the relative error to the widening parameter σ for $ka = 10$ and incident angle $\varphi_0 = 0$; DtN2 (plain), BGT2 (dashed).

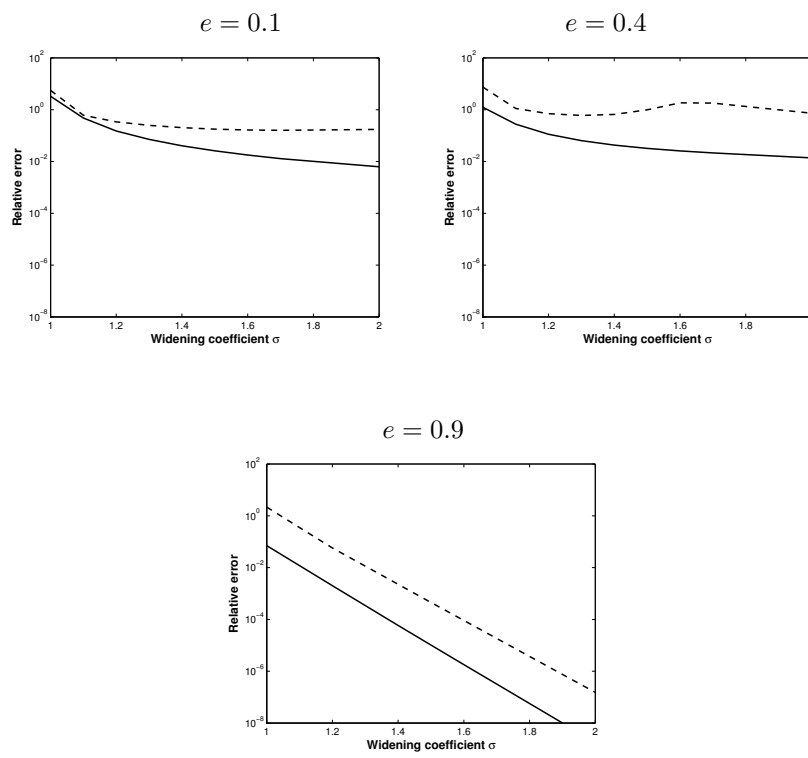


Figure 10: Sensitivity of the relative error to the widening parameter σ for $ka = 10$ and incident angle $\varphi_0 = \frac{\pi}{4}$; DtN2 (plain), BGT2 (dashed).

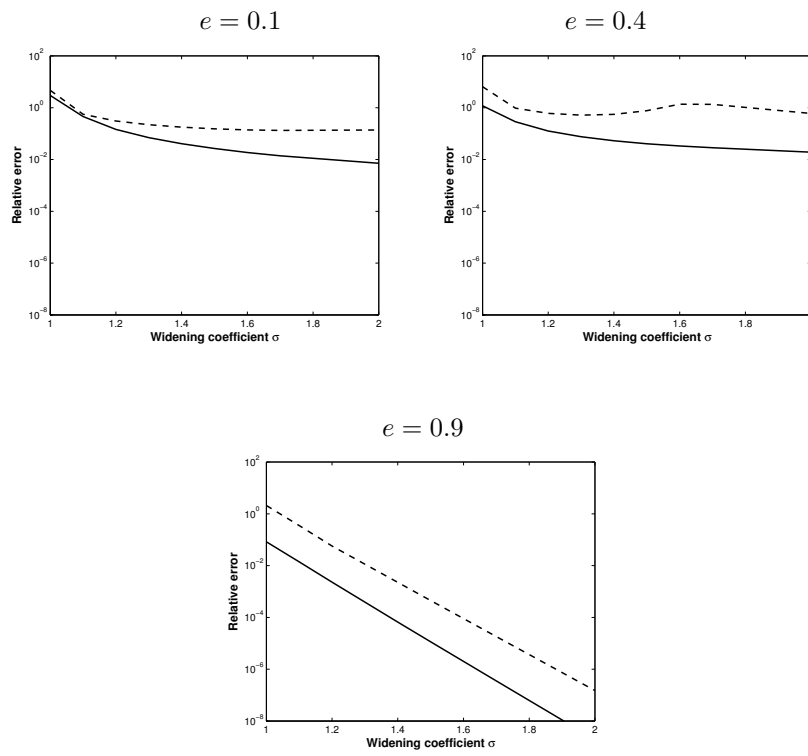


Figure 11: Sensitivity of the relative error to the widening parameter σ for $ka = 10$ and incident angle $\varphi_0 = \frac{\pi}{2}$; DtN2 (plain), BGT2 (dashed).

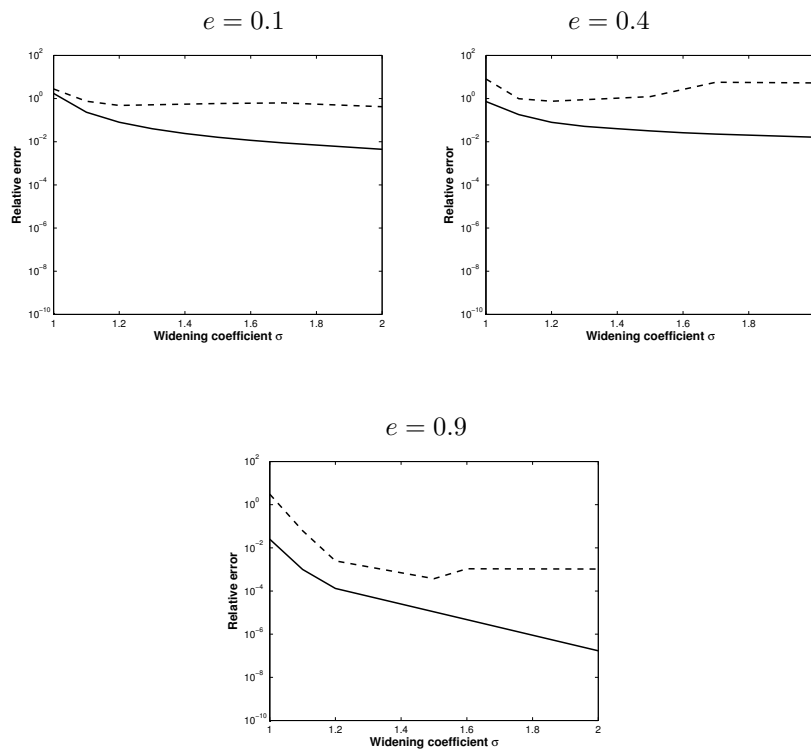


Figure 12: Sensitivity of the relative error to the widening parameter σ for $ka = 20$ and incident angle $\varphi_0 = 0$; DtN2 (plain), BGT2 (dashed).

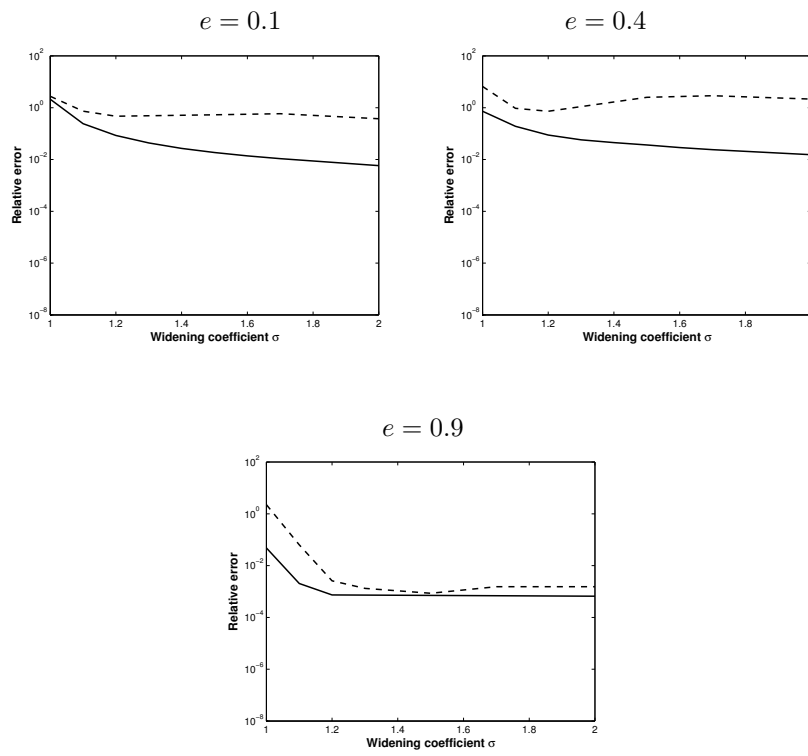


Figure 13: Sensitivity of the relative error to the widening parameter σ for $ka = 20$ and incident angle $\varphi_0 = \frac{\pi}{4}$; DtN2 (plain), BGT2 (dashed).

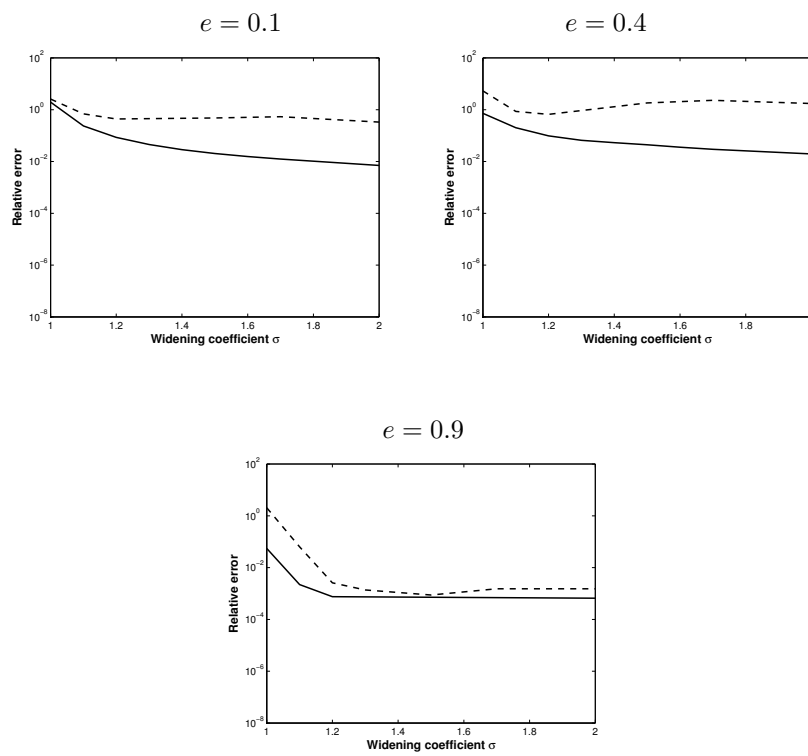


Figure 14: Sensitivity of the relative error to the widening parameter σ for $ka = 20$ and incident angle $\varphi_0 = \frac{\pi}{2}$; DtN2 (plain), BGT2 (dashed).

4 Conclusion

We have performed an analytical study of the performance of the local approximate DtN2 absorbing boundary condition designed for exterior artificial prolate spheroidal-shaped boundaries [4]. We have adopted a domain-based formulation to conduct this analysis in the high frequency regime. The mathematical and numerical analysis demonstrated that the proposed boundary condition is very efficient in the high frequency when employed on elongated boundaries. Indeed, the DtN2 produces little reflections at the exterior boundary that decay faster than $1/(ka_\Gamma)^{15/8}$, while the propagating waves tend to the exact solution. The numerical investigation tends to indicate that it is enough to set the widening coefficient σ at about 1.2 to retain a level of accuracy less than 1%. This result suggests that, in practice, the use of the DtN2 boundary condition incurs relatively small computation domain in order to achieve an acceptable level of accuracy.

Acknowledgments

The authors acknowledge the support by INRIA/CSUN Associate Team Program and by ANR/AHPI research program (Agence Nationale de la Recherche/Analyse Harmonique et Problèmes Inverses). Any opinions, findings, conclusions or recommendations expressed in this material are those of the authors and do not necessarily reflect the views of ANR, CSUN, or INRIA.

Appendix: BGT2 approximate solution

We consider the mixed boundary value problem:

$$\begin{cases} \Delta u^{\text{BGT}} + k^2 u^{\text{BGT}} = 0 & \text{in } \Omega^b \\ u^{\text{BGT}} = -u^{\text{inc}} & \text{on } \Gamma \\ \frac{\partial u^{\text{BGT}}}{\partial \mathbf{n}} = \frac{1}{a_\Sigma \sqrt{1 - e_\Sigma^2 \cos^2 \varphi}} T u^{\text{BGT}} & \text{on } \Sigma \end{cases} \quad (56)$$

where \mathbf{n} is the outward normal to the exterior boundary Σ and T is the second-order local approximate BGT operator expressed in prolate spheroid coordinates as follows [17]:

$$Tu = \sqrt{1 - e_\Sigma^2} \left((ika_\Sigma - 1) u + \frac{1}{2(1 - ika_\Sigma)} \Delta_\Sigma u \right) \quad (57)$$

The approximate scattered field u^{BGT} can be expressed as an infinite series of outgoing modes $R_{mn}^{(3)}(kf, \cosh \xi)$ and incoming modes $R_{mn}^{(4)}(kf, \cosh \xi)$. More specifically, we have (see Eq. (16) p. 233 in [16]):

$$u^{\text{BGT}} = \sum_{m=0}^{+\infty} \sum_{n=m}^{+\infty} \left[d_{mn}^{\text{BGT}} u_{mn}^{(3)}(kf, \cosh \xi, \cos \varphi) + \tau_{mn}^{\text{BGT}} u_{mn}^{(4)}(kf, \cosh \xi, \cos \varphi) \right] \quad (58)$$

where $u_{mn}^{(j)}(kf, \cosh \xi, \cos \varphi)$ are given by Eq. (9).

Similarly to the DtN boundary condition (see Section), the determination of the Fourier coefficients d_{mn}^{BGT} and τ_{mn}^{BGT} requires solving the following 2×2 systems:

$$\begin{cases} d_{mn}^{\text{BGT}} R_{mn|_\Gamma}^{(3)} + \tau_{mn}^{\text{BGT}} R_{mn|_\Gamma}^{(4)} = -d_{mn}^{\text{inc}} R_{mn|_\Gamma}^{(1)} & \text{on } \Gamma \\ d_{mn}^{\text{BGT}} \tilde{\Psi}_{mn|_\Sigma}^{(3)} + \tau_{mn}^{\text{BGT}} \tilde{\Psi}_{mn|_\Sigma}^{(4)} = 0 & \text{on } \Sigma \end{cases} \quad (59)$$

where

$$\tilde{\Psi}_{mn|_\Sigma}^{(j)} = R_{mn|_\Sigma}^{(j)'} - \gamma_{mn} R_{mn|_\Sigma}^{(j)}; \quad j = 3, 4 \quad (60)$$

and the coefficient γ_{mn} is given by

$$\gamma_{mn|_\Sigma} = \frac{\lambda_{mn|_\Sigma} - (e_\Sigma k a_\Sigma)^2}{2(1 - ika_\Sigma)} + 1 - ika_\Sigma \quad (61)$$

The linear system given by Eq.(59) admits a unique solution if and only if the wronskien-like expression given by:

$$\tilde{W}_{mn}^{3,4}(\Gamma, \Sigma) = R_{mn|_\Gamma}^{(3)} \tilde{\Psi}_{mn|_\Sigma}^{(4)} - R_{mn|_\Gamma}^{(4)} \tilde{\Psi}_{mn|_\Sigma}^{(3)} \quad (62)$$

satisfies

$$\tilde{W}_{mn}^{3,4}(\Gamma, \Sigma) \neq 0$$

Under this necessary and sufficient condition, the Fourier coefficients can be expressed as follows:

$$\begin{cases} d_{mn}^{\text{BGT}} = -\frac{d_{mn}^{\text{inc}} \tilde{\Psi}_{mn|\Sigma}^{(4)} R_{mn|\Gamma}^{(1)}}{\widehat{W}_{mn}^{3,4}(\Gamma, \Sigma)} \\ \tau_{mn}^{\text{BGT}} = \frac{d_{mn}^{\text{inc}} \tilde{\Psi}_{mn|\Sigma}^{(3)} R_{mn|\Gamma}^{(1)}}{\widehat{W}_{mn}^{3,4}(\Gamma, \Sigma)} \end{cases} \quad (63)$$

Using the expression of the Fourier coefficients d_{mn}^{inc} of the incident plane wave u^{inc} (see Eq. (8)) together with expression of the Fourier coefficients d_{mn}^{scat} (see Eq. (13)) of the scattered field u^{scat} (see Eq. (11)), we can rewrite Eq. (63) as follows:

$$\begin{cases} d_{mn}^{\text{BGT}} = \frac{\tilde{\Psi}_{mn|\Sigma}^{(4)} R_{mn|\Gamma}^{(3)}}{\widehat{W}_{mn}^{3,4}(\Gamma, \Sigma)} d_{mn}^{\text{scat}} \\ \tau_{mn}^{\text{BGT}} = \frac{\tilde{\Psi}_{mn|\Sigma}^{(3)} R_{mn|\Gamma}^{(3)}}{\widehat{W}_{mn}^{3,4}(\Gamma, \Sigma)} d_{mn}^{\text{scat}} \end{cases} \quad (64)$$

References

- [1] M. ABRAMOVITZ, I. STEGUN, *Handbook of Mathematical Functions with Formulas, Graphs and Mathematical Tables*, Dover Publications, New York, 1972.
- [2] X. ANTOINE, *Fast approximate computation of a time-harmonic scattered field using the On-Surface Radiation Condition method*, IMA J. Appl. Math., 66 (1), 83–110, 2001.
- [3] X. ANTOINE, M. DARBAS, Y.Y. LU, *An improved surface radiation condition for high-frequency acoustic scattering problems*, Comput. Methods Appl. Mech. Engrg., 195 (33-36), 4060–4074, 2006.
- [4] H. BARUCQ, R. DJELLOULI, A. SAINT-GUIRONS, *Performance assessment of a new class of local absorbing boundary conditions for elliptical-shaped boundaries*, Applied Numerical Mathematics, 59, 1467–1498, 2009.
- [5] A. BAYLISS, M. GUNZBURGER, E. TURKEL, *Boundary conditions for the numerical solution of elliptic equations in exterior regions*, SIAM J. Appl. Math., 42 (2), 430–451, 1982.
- [6] J.J. BOWMAN, T.B.A. SENIOR, P.L.E. USLENGHI, *Electromagnetic and acoustic scattering by simple shapes*, North-Holland Publishing company, Amsterdam, 1969.
- [7] D. COLTON, R. KRESS, *Integral Equations in Scattering Theory*, Pure and Applied Mathematics, John Wiley and Sons, New York, 1983.
- [8] M. DARBAS, *Préconditionneurs analytiques de type Calderon pour les formulations intégrales des problèmes de diffraction d’ondes*, Thèse de Doctorat, Université de Toulouse 1 et Toulouse 3, INSA Toulouse, 2004.
- [9] C. FLAMMER, *Spheroidal Functions*, Stanford University Press, Stanford, CA, 1957.
- [10] D. GIVOLI AND J.B. KELLER, *Nonreflecting boundary conditions for elastic waves*, Wave Motion, 12(3), 261–279, 1990.
- [11] I. HARARI, T.J.R. HUGHES, *Analysis of continuous formulations underlying the computation of time-harmonic acoustics in exterior domains*, Comput. Methods Appl. Mech. Engrg., 97 (1), 103–124, 1992.
- [12] G.A. KRIEGSMANN, A. TAFLOVE, K.R. UMASHANKAR, *A new formulation of electromagnetic wave scattering using an on-surface radiation boundary condition approach*, IEEE Trans. Antennas and Propagation, 35 (2), 153–161, 1987.
- [13] F. MAGOULÈS, *Computational Methods for Acoustics Problems*, Saxe-Coburg Publications, 2008.

- [14] M. MEDVINSKY, E. TURKEL, U. HETMANIUK, *Local absorbing boundary conditions for elliptical shaped boundaries*, J. Comput. Phys., in press, 2008.
- [15] J. MEIXNER, F.W. SCHAFLE, *Matieusche funktionen and spharoidfunktionen*, Springer Verlag, Berlin, 1954.
- [16] M. NIGSCH, *Numerical studies of time-independent and time-dependent scattering by several elliptical cylinders*, Journal of Computational and Applied Mathematics, 204, 231-241, 2007.
- [17] R.C. REINER, R. DJELLOULI, I. HARARI, *The performance of local absorbing boundary conditions for acoustic scattering from elliptical shapes*, Comput. Methods Appl. Mech. Engrg, 195, 3622-3665, 2006.
- [18] R.C. REINER, R. DJELLOULI, *Improvement of the performance of the BGT2 condition for low frequency acoustic scattering problems*, Wave Motion, 43, 406-424, 2006.
- [19] A-G. SAINT-GUIRONS, *Construction et analyse de conditions absorbantes de type Dirichlet-to-Neumann pour des frontières ellipsoïdales*, Thèse de Doctorat, Université de Pau et des Pays de l'Adour, 2008.
- [20] T.B.A. SENIOR, *Scalar diffraction by a prolate spheroid at low frequencies*, Canad. J. Phys., 38 (7), 1632-1641, 1960.
- [21] J.A. STRATTON, *Electromagnetic theory*, McGraw-Hill, New York, 1941.
- [22] E. TURKEL, *Boundary Conditions and Iterative Schemes for the Helmholtz Equation in Unbounded Regions*, In: Computational Methods for Acoustics Problems, F. Magoulès (ed.), Saxe-Coburg Publications, , 127-158, 2009 .

Contents

1	Introduction	3
2	Preliminaries	4
2.1	Nomenclature and assumption	4
2.2	The acoustic scattering problem	5
2.3	Bounded domain-based formulation	6
3	Analytical study	7
3.1	Existence and uniqueness of the approximate solution	7
3.1.1	Mathematical results	7
3.1.2	Illustrative numerical results	12
3.2	Accuracy of the approximate scattered field	15
3.2.1	Mathematical results	15
3.2.2	Illustrative numerical results	18
4	Conclusion	32



Centre de recherche INRIA Bordeaux – Sud Ouest
Domaine Universitaire - 351, cours de la Libération - 33405 Talence Cedex (France)

Centre de recherche INRIA Grenoble – Rhône-Alpes : 655, avenue de l'Europe - 38334 Montbonnot Saint-Ismier
Centre de recherche INRIA Lille – Nord Europe : Parc Scientifique de la Haute Borne - 40, avenue Halley - 59650 Villeneuve d'Ascq
Centre de recherche INRIA Nancy – Grand Est : LORIA, Technopôle de Nancy-Brabois - Campus scientifique
615, rue du Jardin Botanique - BP 101 - 54602 Villers-lès-Nancy Cedex
Centre de recherche INRIA Paris – Rocquencourt : Domaine de Voluceau - Rocquencourt - BP 105 - 78153 Le Chesnay Cedex
Centre de recherche INRIA Rennes – Bretagne Atlantique : IRISA, Campus universitaire de Beaulieu - 35042 Rennes Cedex
Centre de recherche INRIA Saclay – Île-de-France : Parc Orsay Université - ZAC des Vignes : 4, rue Jacques Monod - 91893 Orsay Cedex
Centre de recherche INRIA Sophia Antipolis – Méditerranée : 2004, route des Lucioles - BP 93 - 06902 Sophia Antipolis Cedex

Éditeur
INRIA - Domaine de Voluceau - Rocquencourt, BP 105 - 78153 Le Chesnay Cedex (France)
<http://www.inria.fr>
ISSN 0249-6399